

## Article

# Hydrogel of HEMA, NVP, and Morpholine-Derivative Copolymer for Sulfate Ion Adsorption: Behaviors and Mechanisms

Jing Zhao <sup>1</sup>, Haitao Liu <sup>2,\*</sup>, Wenwen Chen <sup>3</sup>, Yu Jian <sup>3,\*</sup>, Guoyong Zeng <sup>3</sup> and Zhenyu Wang <sup>4,\*</sup>

<sup>1</sup> Laboratory of Organic Solid Waste Treatment and Recycling, College of Materials Science and Engineering, Henan Institute of Technology, Xinxiang 453003, China

<sup>2</sup> College of Chemistry and Materials Engineering, Wenzhou University, Wenzhou 325035, China

<sup>3</sup> Department of Chemistry, Lishui University, Lishui 323000, China

<sup>4</sup> Department of Environmental Engineering, College of Ecology, Lishui University, Lishui 323000, China

\* Correspondence: 00111051@wzu.edu.cn (H.L.); yujian\_79@126.com (Y.J.); lsxy9552@163.com (Z.W.)

**Abstract:**  $\text{SO}_4^{2-}$ -containing compounds are widely present in wastewater generated from various industries and mining industries, such as slag leachate, pulp and paper wastewater, modified starch wastewater, etc. When the concentration of  $\text{SO}_4^{2-}$  is too high, it will not only be corrosive to metal equipment but also accumulate in the environmental media. Based on this, a novel cationic hydrogel HNM was synthesized in this study by introducing morpholine groups into the conventional hydrogel HEMA–NVP system for the adsorption of  $\text{SO}_4^{2-}$  in aqueous solutions. Characterizations by Fourier transform infrared (FTIR) spectroscopy and X-ray photoelectron spectroscopy (XPS) indicated that morpholine groups had been introduced into the as-synthesized hydrogels. The scanning electron microscope (SEM) characterization results show that the introduction of morpholine groups changed the surface of the hydrogel from micron-scale wrinkles to nanoscale gaps, increasing the contact area with the solution. The results of static water contact angle (WCA), equilibrium water content (EWC), and  $\text{SO}_4^{2-}$  adsorption capacity show that the introduction of morpholine groups not only further improved the equilibrium water content and hydrophilicity of the hydrogel but also greatly improved the  $\text{SO}_4^{2-}$  adsorption capacity of the hydrogel, with the maximum  $\text{SO}_4^{2-}$  adsorption amount of 21.59 mg/g, which was much higher than that of the hydrogel without morpholine groups of 5.15 mg/g. Further studies found that the adsorption of  $\text{SO}_4^{2-}$  on the hydrogel HNM was pH-dependent, and acidic conditions were favorable for the adsorption. Therefore, the introduction of morpholine groups greatly enhanced the ability of conventional HEMA–NVP hydrogels to remove  $\text{SO}_4^{2-}$  from aqueous solutions.



**Citation:** Zhao, J.; Liu, H.; Chen, W.; Jian, Y.; Zeng, G.; Wang, Z. Hydrogel of HEMA, NVP, and Morpholine-Derivative Copolymer for Sulfate Ion Adsorption: Behaviors and Mechanisms. *Molecules* **2023**, *28*, 984. <https://doi.org/10.3390/molecules28030984>

Academic Editors: Afang Zhang and Jianxun Ding

Received: 5 December 2022

Revised: 24 December 2022

Accepted: 9 January 2023

Published: 18 January 2023



**Copyright:** © 2023 by the authors. Licensee MDPI, Basel, Switzerland. This article is an open access article distributed under the terms and conditions of the Creative Commons Attribution (CC BY) license (<https://creativecommons.org/licenses/by/4.0/>).

## 1. Introduction

Sulfate ions are widely distributed in surface water, groundwater, and industrial wastewater, such as acid mine, pharmaceutical, printing, and dyeing wastewater [1]. Although sulfate ions are usually considered nontoxic, they are potentially harmful to organisms and the environment. High concentrations of sulfate ions in water can lead to an imbalance in the natural sulfur cycle in ecosystems and can be hazardous to human health when ingested in excess over time [2,3]. In addition, sulfate ions in the environment can also cause serious damage to buildings. For example, the hydration products in concrete structures in buildings react with sulfate ions to form gypsum and calcium alumina, leading to the expansion and cracking of concrete structures, reduction of strength, and ultimately structural damage [4,5]. Therefore, efforts to reduce or eliminate sulfate ions in the environment are important.

Currently, the main techniques for eliminating sulfate ions include chemical precipitation, ion exchange, biological treatment, adsorption, and membrane filtration [6]. However, chemical precipitation and ion exchange methods are prone to problems, such as water deterioration and soil acidification, and biological treatment and membrane filtration treatment are more expensive, so these methods are somewhat limited in practical application [7]. Adsorption methods have the advantages of high removal efficiency, stable performance, simple operation, and high cost-effectiveness and have attracted increasing research attention worldwide [8,9]. Currently, commonly used adsorption materials include metal–organic frameworks (MOFs) [10], carbon-based materials [11], and zeolites [12], but the performance of these materials needs further improvement. For example, carbon-based materials and zeolites have limitations with low adsorption capacity and weak selectivity and stability [13]. Although MOF materials have good absorption properties, the disadvantages, such as complicated preparation, high energy cost, and unstable aqueous solution, limit their potential applications [14]. Therefore, exploring new adsorbent materials with high performance, easy operation, and low cost has become an attractive research topic.

In recent years, hydrogels have attracted much attention because of their unique physicochemical properties. Hydrogels have a three-dimensional network structure, which can absorb large amounts of water or other aqueous fluids and maintain their integrity by physical (ionic, hydrogen, or van der Waals bonds) or chemical (covalent bonds) cross-linking [15]. Moreover, hydrogels can adsorb and trap ions and molecules through a porous network structure capable of physicochemical interactions with molecules and ions in aqueous fluids. In addition, hydrogels respond to environmental stimuli (pH, salt concentration, temperature, etc.) under weak changes in the stimuli [16–18]. Therefore, their wide application in biotechnology, medicine, agriculture, food industry, and water purification has attracted great interest in the last decades [19,20]. However, pure hydrogels have no specific sites and poor adsorption of sulfate ions.

The adsorption performance of hydrogels for anions can be greatly improved by incorporating various organic materials and metal ions into the hydrogels. For example, Fang prepared a new high-capacity cationic hydrogel adsorbent from an aqueous medium by condensation with triethylenetetramine, acetone, and formaldehyde. The hydrogel has a high cationic charge density and abundant functional groups and has a high adsorption uptake rate for anionic dyes [21]. Morpholine is a six-membered cyclic compound containing nitrogen and oxygen atoms. Due to their biological and pharmacological properties, morpholines are used in many applications, such as antioxidant [22] and anti-inflammatory [23]. In addition, morpholine groups have a positive charge, and their electrochemical properties are remarkable, and there are many studies on the electrochemical applications of compounds containing morpholine groups [24–27]. However, to our knowledge, there is no literature on the synthesis, characterization, and application of morpholine groups in hydrogel materials for anion adsorption.

In this paper, copolymer hydrogels with different contents of 2-morpholine ethanol monomer (HEMA–NVP–Mor) were prepared by introducing 2-morpholine ethanol as a copolymer monomer into the conventional HEMA–NVP copolymer hydrogel system. The structural morphology, surface chemistry, and thermal stability of the prepared hydrogels were characterized using FTIR, SEM, XPS, TGA, and other analytical methods. The effects of the content of 2-morpholine ethanol monomer, the initial pH value of the solution, the adsorption concentration, and the adsorption time on the adsorption performance of the materials were further investigated. The experimental results show that the introduction of morpholine groups increased the specific surface area of the hydrogel and improved the adsorption capacity of sulfate ions. In addition, the adsorption capacity of the polymeric materials for sulfate at different pH values was also investigated. This study not only promotes the research of using modified hydrogels to treat sulfate ions in wastewater but also provides ideas for the removal of other anionic pollutants.

## 2. Results and Discussion

To identify the functional groups and their chemical composition characterization, FTIR was used for the analysis. The infrared spectra of MCAEM monomer, HMN-1, and HMN-4 were tested and analyzed as shown in Figure 1. In curve (a),  $864\text{ cm}^{-1}$  and  $868\text{ cm}^{-1}$  are the vibrational peaks of C–N on the morpholine ring in 2-morpholine ethanol;  $1625\text{ cm}^{-1}$  and  $1120\text{ cm}^{-1}$  are the vibrational peaks of C=O and C–O of the ester group on HEMA, and the characteristic peak at  $1653\text{ cm}^{-1}$  is attributed to the generated imino group. In curve (b), the characteristic peaks at  $1725\text{ cm}^{-1}$  and  $1653\text{ cm}^{-1}$  are attributed to the ester group in HEMA and the acyl group in NVP, and the  $1638\text{ cm}^{-1}$  vibrational peak of C=C has disappeared, indicating that HEMA and NVP have been polymerized into hydrogels. In curve (c), compared with curve (b), a vibrational peak of  $868\text{ cm}^{-1}$  (C–N of the morpholine ring in MCAEM) appears, indicating that MCAEM has successfully polymerized with HEMA and NVP. The chemical properties of the surface of the hydrogel HMN-4 sample were further analyzed by XPS, and the test results are shown in Figure 2. The XPS broad spectrum showed three characteristic signal peaks of Cls (283 eV), O1s (530 eV), and N1s (398 eV) on the surface of the hydrogel, indicating the presence of C, O, and N elements on the surface of the hydrogel, which is consistent with the FTIR test results.

The surface morphologies of the synthesized hydrogel materials HNM-1 and HNM-4 were characterized by SEM, and the results are shown in Figure 3. As shown in Figure 3a, the surface of HNM-1 exhibits a micron-sized furrow morphology, and some granular bumps exist on the surface. When the surface of HNM-1 was further enlarged, it showed an obviously folded morphology (as shown in Figure 3b). While the surface of HNM-4 has some granular bumps, it shows a smoother and flatter shape overall, as shown in Figure 3c. When the surface of HNM-4 is further magnified, there are nanoscale gaps on the surface of HNM-4, and these gaps are beneficial to increase the contact area of the hydrogel. As seen in the figure, the addition of the MCAEM monomer enhances the flatness of the surface of the hydrogel material, reduces the roughness of the surface, and improves the contact area with the solution.

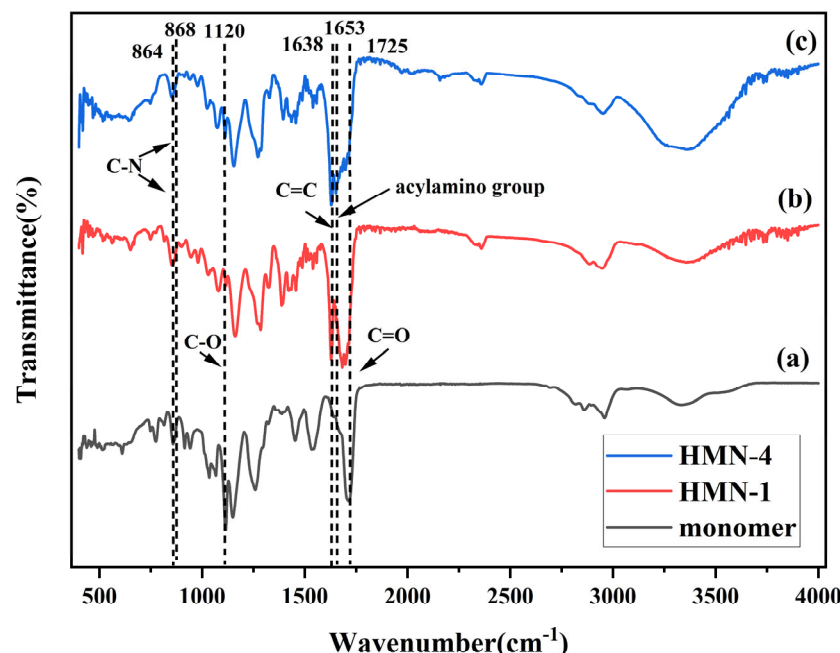


**Figure 1.** FTIR spectra of (a) monomer, (b) HMN-1, and (c) HMN-4.

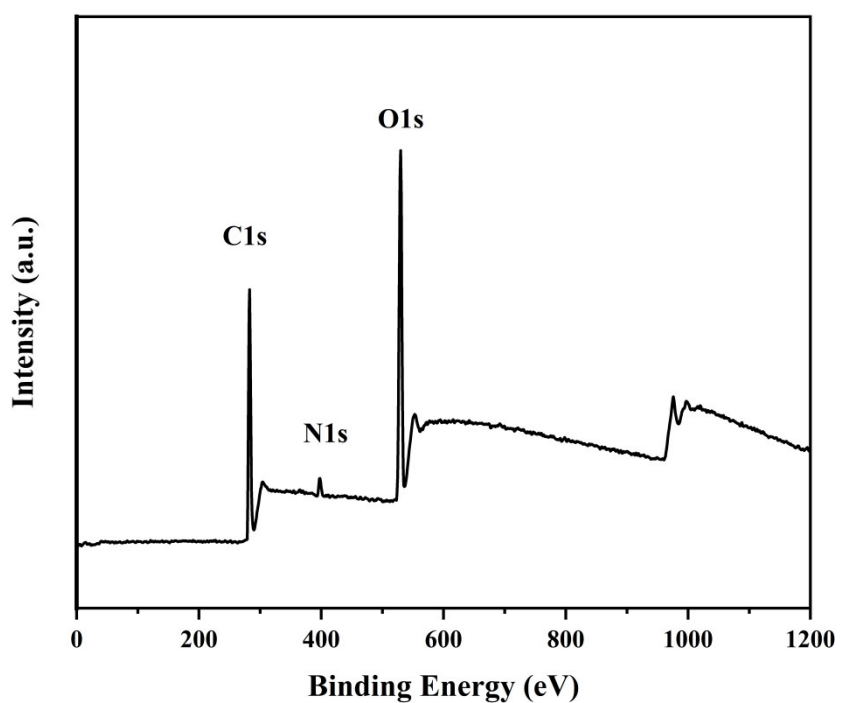


**Figure 2.** XPS spectra of the hydrogel HMN-4.

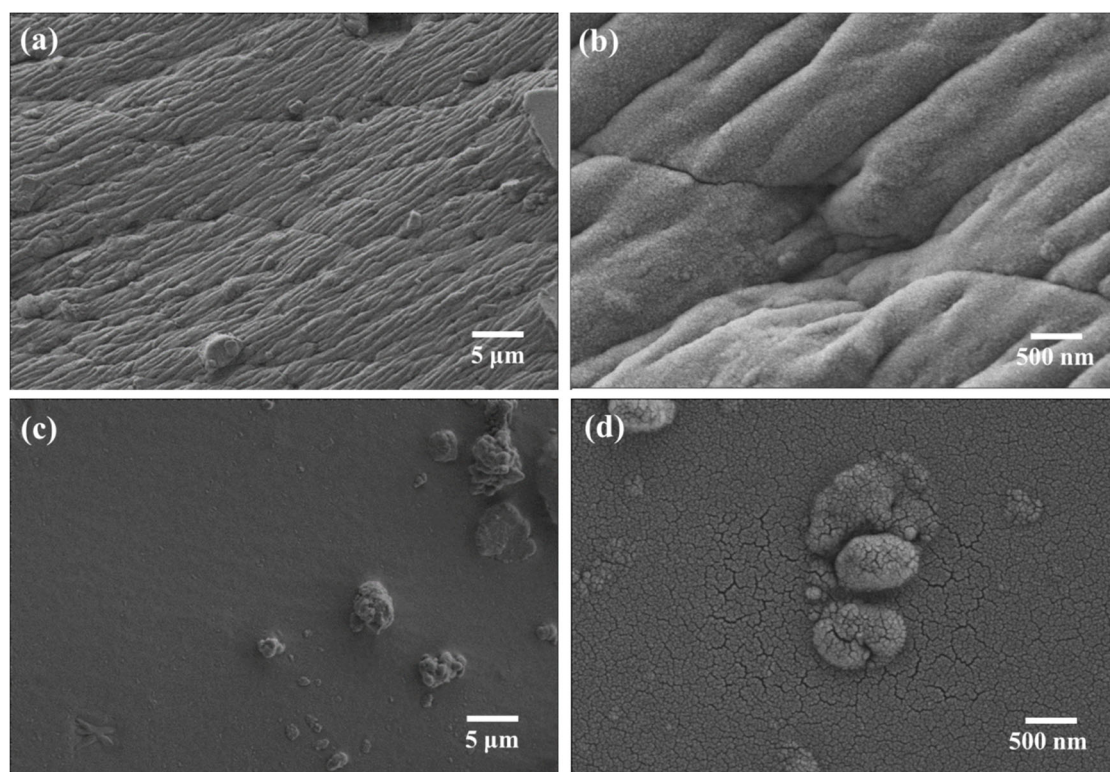


**Figure 3.** SEM images of (a,b) HMN-1 and (c,d) HMN-5.

The effect of copolymeric monomers on the EWC of hydrogels is shown in Figure 4. As seen in the figure, as the content of the MCAEM monomer increased, the EWC value of the synthesized hydrogel material then increased until saturation, from 69.15% for HNM-1 to 86.59 % for HNM-5. This is mainly because the MCAEM monomers are hydrophilic monomers, so as the proportion of MCAEM in the synthesized hydrogel increases, the

ability of the material to adsorb water molecules inside the material increases, leading to an increase in the EWC value of the material. When the water content inside the material reaches a certain value, the ability to accommodate water molecules in the network structure of the material reaches saturation, so the EWC value of the hydrogel material no longer increases as the proportion of MCAEM in the synthetic hydrogel increases further.

The measured static contact angles of HNM-1 and HNM-4 are shown in Figure 5. The WCA of HNM-1 without the MCAEM monomer was  $65.49^\circ$  (Figure 5a), which indicates the good hydrophilicity of the unmodified hydrogel. In contrast, the WCA of the HNM-4 hydrogel surface decreased to  $51.96^\circ$  (Figure 5b), which indicated the enhanced hydrophilicity of the synthetic hydrogel with the addition of the MCAEM monomer and the enhanced wettability of the material surface. The static contact angle measurements were consistent with the EWC-worthy measurements.

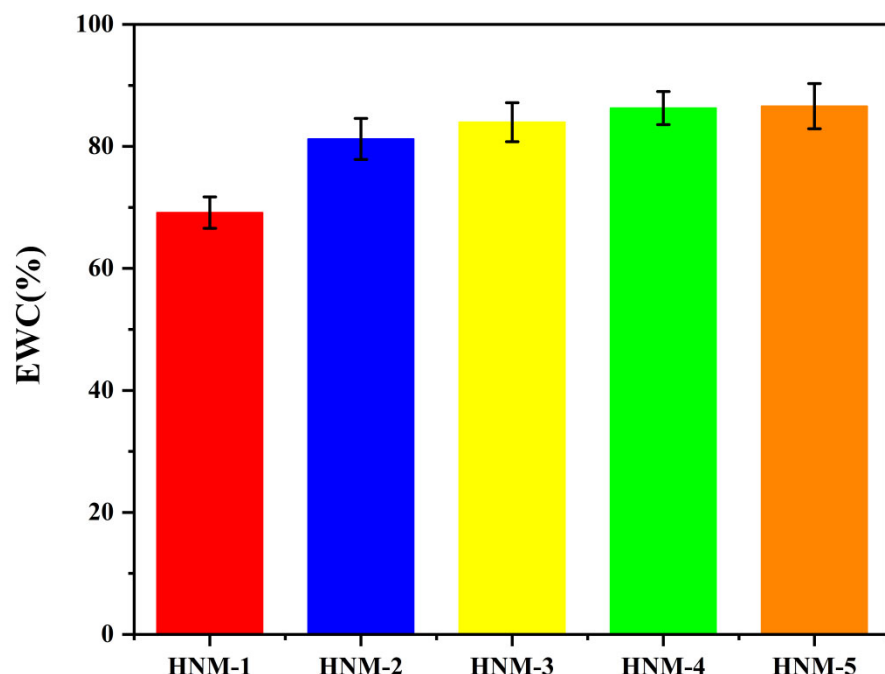


**Figure 4.** Equilibrium water content of HNM-1, HNM-2, HNM-3, HNM-4, and HNM-5.

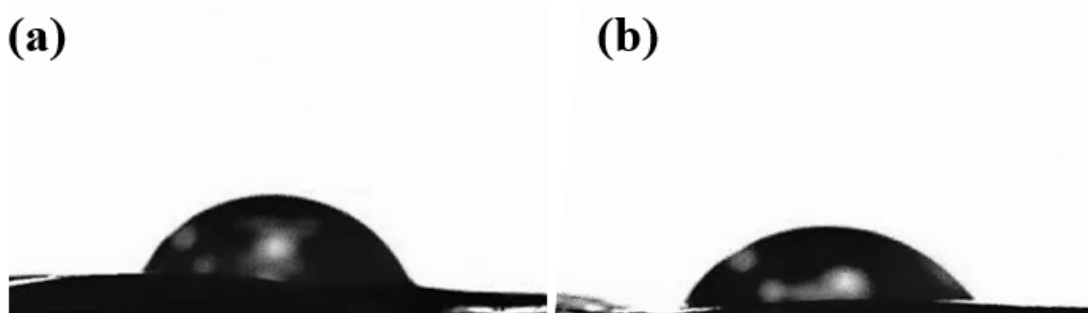


**Figure 5.** Static contact angle of (a) HNM-1 and (b) HNM-4 is  $65.49^\circ$  and  $51.96^\circ$ , respectively.

The effect of the variation of the MCAEM content in the polymer on the adsorption effect of the hydrogels was investigated, and the results are shown in Figure 6. All four hydrogels with the added MCAEM monomer showed good adsorption capacity for sulfate ions. Among them, HNM-4 showed the best adsorption effect with the maximum adsorption amount of  $21.59\text{ mg/g}$  for sulfate, while HNM-1, which did not contain the MCAEM monomer, showed the maximum adsorption amount of only  $5.15\text{ mg/g}$ . The results may be due to the presence of the MCAEM branched chains in the polymer network,

which provided positively charged adsorption sites and easier adsorption of sulfate ions into the hydrogel network. The decrease in the adsorption amount after reaching the maximum value on the HNM-4 surface may be due to the large number of the MCAEM branched chains crossing with other branched chains, reducing the space of pores in the three-dimensional network of the hydrogel, thus leading to a decrease in the maximum adsorption capacity of the hydrogel for sulfate ions.

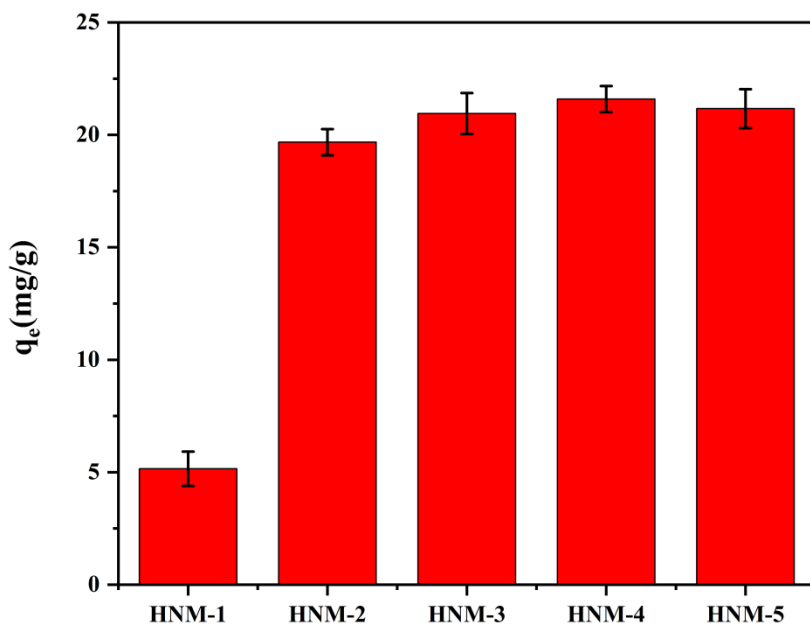


**Figure 6.** Adsorption capacities of HNM-1, HNM-2, HNM-3, HNM-4, and HNM-5 for  $\text{SO}_4^{2-}$ .

The adsorption performance of a hydrogel adsorbent depends largely on the pH of the solution, because pH can affect the surface charge of the adsorbent and thus the adsorption capacity of the hydrogel. In the presence of hydrogels, the initial pH of the solution changes, and when the difference between the equilibrium pH and the initial pH is zero, the pH of the solution is called the pHPZC at the point of zero charge. Therefore, when the solution pH is equal to the pHPZC, the hydrogel will remain neutral, as shown in Table 1, where the pHPZC values of HNM-1 to HNM-5 were tested. The sulfate ion adsorption capacity of the hydrogel HNM-4 was further tested at a different initial pH, and the results are shown in Figure 7. HNM-4 hydrogel showed a pH-dependent adsorption behavior, and the adsorption capacity is greater at a low pH and decreases with increasing pH. When the solution pH is less than pHPZC, the surface of the hydrogel becomes positively charged, and  $\text{SO}_4^{2-}$  is easily captured by the hydrogel through electrostatic attraction. When the  $\text{pH} > \text{pHPZC}$ , the charge on the hydrogel surface reverses from positive to negative with increasing pH, leading to an increase in electrostatic repulsion and a decrease in  $\text{SO}_4^{2-}$  uptake. In addition, at a high pH, the large amount of  $\text{OH}^-$  ions present in the solution compete with sulfate ions for the active adsorption sites on the HNM-4 surface, which also leads to a decrease in the sulfate adsorption capacity. Therefore, the adsorption capacity of sulfate ions is higher in acidic environments.

**Table 1.** The pHPZC value of HNM-1, HNM-2, HNM-3, HNM-4, and HNM-5.

	HNM-1	HNM-2	HNM-3	HNM-4	HNM-5
pHPZC	7.59	6.73	6.68	6.66	6.61

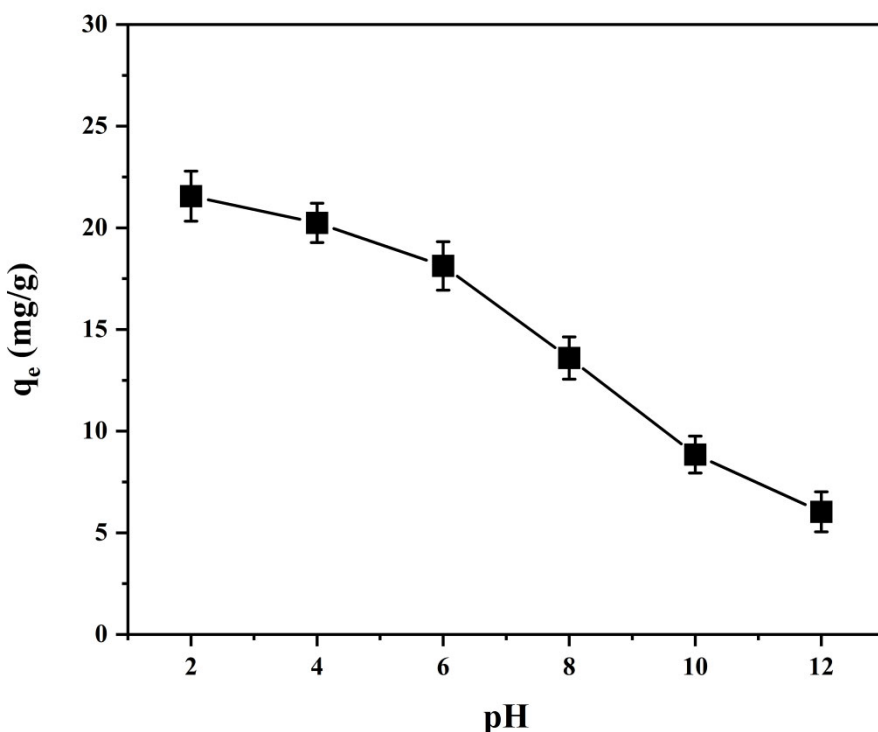


**Figure 7.** Effect of pH on the  $\text{SO}_4^{2-}$  adsorption capacity of HNM-4.

The kinetics of the adsorption of hydrogel HNM-4 were studied and analyzed. The sulfate ion adsorption process can be divided into two stages: the rapid increase stage and the near equilibrium stage. The equilibrium time of sulfate ion adsorption was about 240 min, and the equilibrium adsorption amount was 21.53 mg/g, as shown in Figure 8a. In contrast, ion exchange resins were often used to adsorb sulfate ions. However, its affinity for water was far less than that of hydrogels. Therefore, it was difficult for sulfate ions to diffuse in the adsorbent with water, resulting in poor adsorption capacity [28,29]. At the beginning of 60 min, the adsorption amount of  $\text{SO}_4^{2-}$  increased rapidly with time, and the adsorption rate was very fast, because the active site (-OH) on the surface of HNM-4 was occupied rapidly by  $\text{SO}_4^{2-}$  in water, and this was the rapid increase stage. A total of 120 min later, the active site on the surface of HNM-4 gradually approached saturation, and the adsorption rate decreased, resulting in the  $\text{SO}_4^{2-}$  adsorption capacity. After 120 min, the active sites on the HNM-4 surface gradually approached saturation, and the adsorption rate decreased, resulting in the slow growth of  $\text{SO}_4^{2-}$  adsorption capacity, and the kinetic curve tends to level off, which is close to the equilibrium stage. To further explore the kinetic characteristics of adsorption, pseudo-first-order and pseudo-second-order models were applied to fit the adsorption kinetic data. The kinetic equations are shown below.

$$\text{Pseudo-first-order equation : } \frac{dq_t}{dt} = k_1(q_e - q_t)$$

$$\text{Pseudo-second-order equation : } \frac{dq_t}{dt} = k_2(q_e - q_t)^2$$

where  $q_t$  (mg/g) and  $q_e$  (mg/g) are the adsorption amounts of sulfate ions at time  $t$  and equilibrium, respectively.  $k_1$  ( $\text{min}^{-1}$ ) and  $k_2$  ( $\text{g}/\text{mg}/\text{min}$ ) are the rate constants of the pseudo-first-order and pseudo-second-order models, respectively. The analytical results of the pseudo-first-order and pseudo-second-order models are shown in Figures 8b and 8c, respectively, and the relevant parameters are listed in Table 2. The fitting results show that the kinetics of HNM-4 adsorption on sulfate ions follow the pseudo-second-order model more, and its correlation coefficient ( $R_2$ ) is close to 1.0, which indicates that the rate control of the adsorption process is a chemical reaction process.

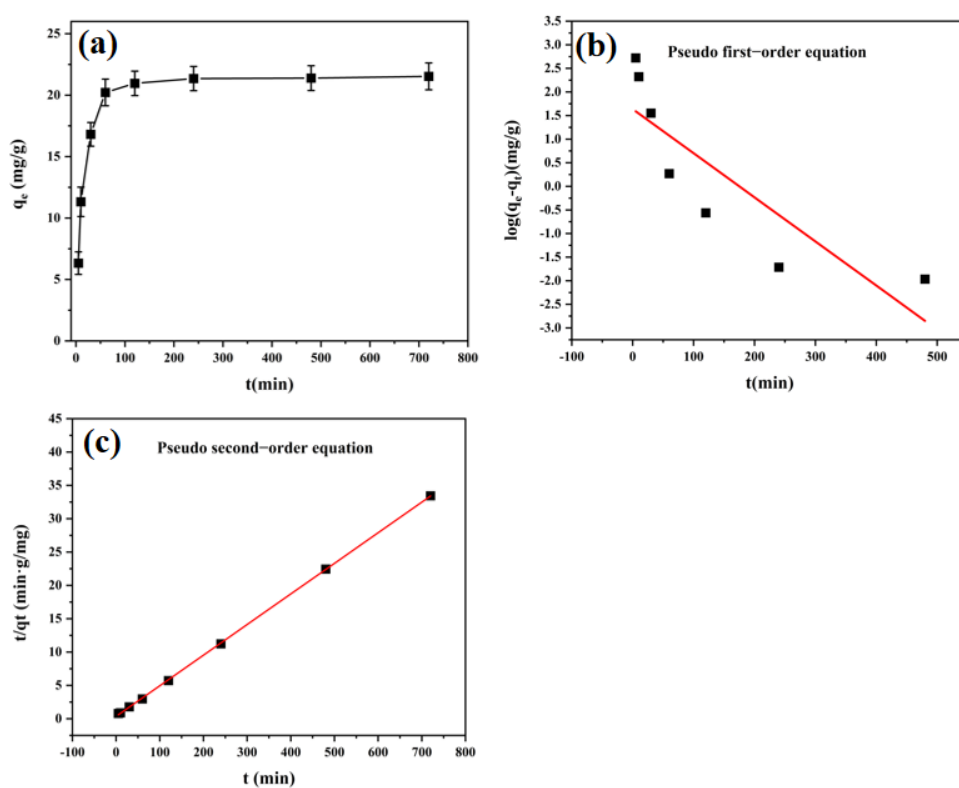


**Figure 8.** (a) Adsorption isotherm, (b) pseudo-first-order model, and (c) pseudo-second-order model of HNM-4.

**Table 2.** Adsorption kinetic model parameters and correlation coefficients ( $R^2$ ) for  $\text{SO}_4^{2-}$  adsorption by HNM-4.

$q_{e,\text{exp}}$ (mg/g)	Pseudo-First-Order Equation			Pseudo-Second-Order Equation		
	$q_{e,\text{Cal}}$ (mg/g)	$k_1$ (min $^{-1}$ )	$R^2$	$q_{e,\text{Cal}}$ (mg/g)	$k_2$ (g·mg $^{-1} \cdot \text{min}^{-1}$ )	$R^2$
21.53	5.138	-0.00935	0.7318	21.79	0.0459	0.9989

The equilibrium adsorption of HNM-4 was studied under different initial concentrations of sulfate ions, and the results are shown in Figure 9. The results show that the initial concentration of sulfate ions plays an important role in the uptake of sulfate ions by the hydrogel. It is clear from Figure 9 that the equilibrium sulfate ion adsorption increases as the initial concentration of sulfate ion increases from 50 to 250 mg/L. The higher the initial concentration of sulfate ions, the higher the uptake of sulfate ions, which is due to the strong electrostatic interaction between the anionic sulfate ion group and the hydrogel with acidic pH. This is because the higher concentration of the solution provides a stronger driving force for the mass transfer of sulfate ions between the aqueous–solid phase. Therefore, a high concentration of sulfate ion solution facilitates the adsorption uptake by the adsorbent. Such behavior has been reported in the literature [30,31].

The adsorption process of sulfate ions was further investigated by fitting the results of the HNM-4 equilibrium adsorption tests for different initial concentrations of sulfate ions using the Freundlich as well as the Langmuir adsorption isotherm curves. The Freundlich and Langmuir equations are shown below.

$$\text{Langmuir model : } q_e = \frac{Q_{\max} K_L C_e}{1 + K_L C_e}$$

$$\text{Freundlich model : } q_e = K_f (C_e)^n$$

where  $Q_e$  (mg/g) and  $C_e$  (mg/L) are the equilibrium adsorption amount and sulfate ion concentration at equilibrium, respectively,  $Q_{\max}$  (mg/g) is the maximum adsorption capacity,  $K_l$  (L/mg) and  $K_f$  ((mg/g)(L/mg) $^{1/n}$ ) are the Langmuir and Freundlich constants, respectively, and  $n$  is the Freundlich linear constant.

Based on the comparison of the calculated correlation coefficient ( $R^2$ ) values, the Langmuir model is more consistent with the experimental data, which indicates that monolayer adsorption may have occurred. The adsorption of HNM-4 on sulfate ions increased with increasing concentration of sulfate ions until the adsorption equilibrium, which is because the binding probability of HNM-4 adsorption sites increased with the initial concentration of sulfate ions. The adsorption amount reached the maximum value at the concentration of 150–200 mg/L of sulfate ions, and the adsorption amount gradually reached equilibrium at the concentration of 200–250 mg/L of sulfate ions. As shown in Table 3, the fitting coefficient  $R^2$  of the Langmuir isotherm model was the largest, so the adsorption reaction process was more suitable to be described by the Langmuir isotherm model, which indicated that the adsorption of sulfate ions by HNM-4 belonged to monolayer adsorption.

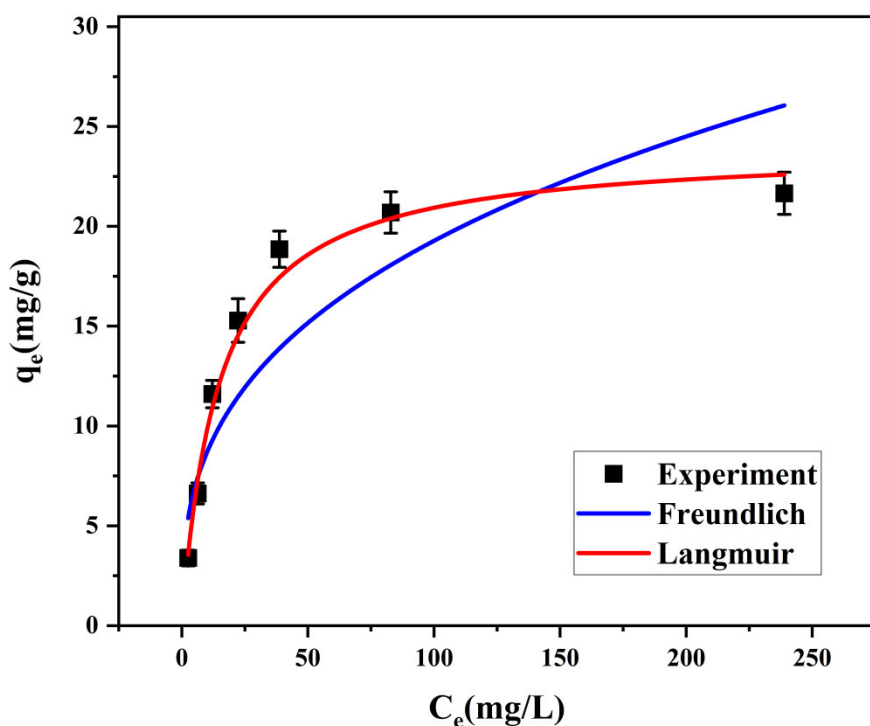


**Figure 9.** Adsorption isotherm, Langmuir isotherm, and Freundlich of HNM-4.

**Table 3.** Adsorption isotherm model parameters and correlation coefficients ( $R^2$ ) for  $\text{SO}_4^{2-}$  adsorption by HNM-4.

Equation	Parameter 1	Parameter 2	$R^2$
Langmuir	$K_l = 0.0690$	$Q_{\max} = 23.960$	0.993
Freundlich	$K_f = 3.913$	$N = 0.346$	0.849

An important property of adsorbent is its reusability. Figure 10 shows the variation trend of  $\text{SO}_4^{2-}$  adsorption capacity and desorption rate in the regeneration cycle of HNM-4. As shown in the figure, after five adsorption–desorption cycles, the adsorption capacity of  $\text{SO}_4^{2-}$  of HNM-4 decreased from 21.49 mg/g to 18.33 mg/g, and the desorption rate decreased from 89% to 83%. The adsorption capacity and desorption rate of the regenerated HNM-4 decreased, but the desorption rate remained above 80%, which also indicated

the potential of the reuse of the adsorbent HNM-4. One of the reasons for the decreased desorption rate of the adsorbents is that the bound  $\text{SO}_4^{2-}$  cannot be desorbed, resulting in the inability to continue adsorption of  $\text{SO}_4^{2-}$  [32]. Therefore, the adsorption site of the hydrogel adsorbent was increased to improve the adsorption capacity after regeneration. In addition, the morpholine group was polymerized in the main chain of hydrogel, which avoids the decrease in  $\text{SO}_4^{2-}$  adsorption capacity caused by the loss of active sites. Therefore, the hydrogel prepared in this study has excellent reusability.

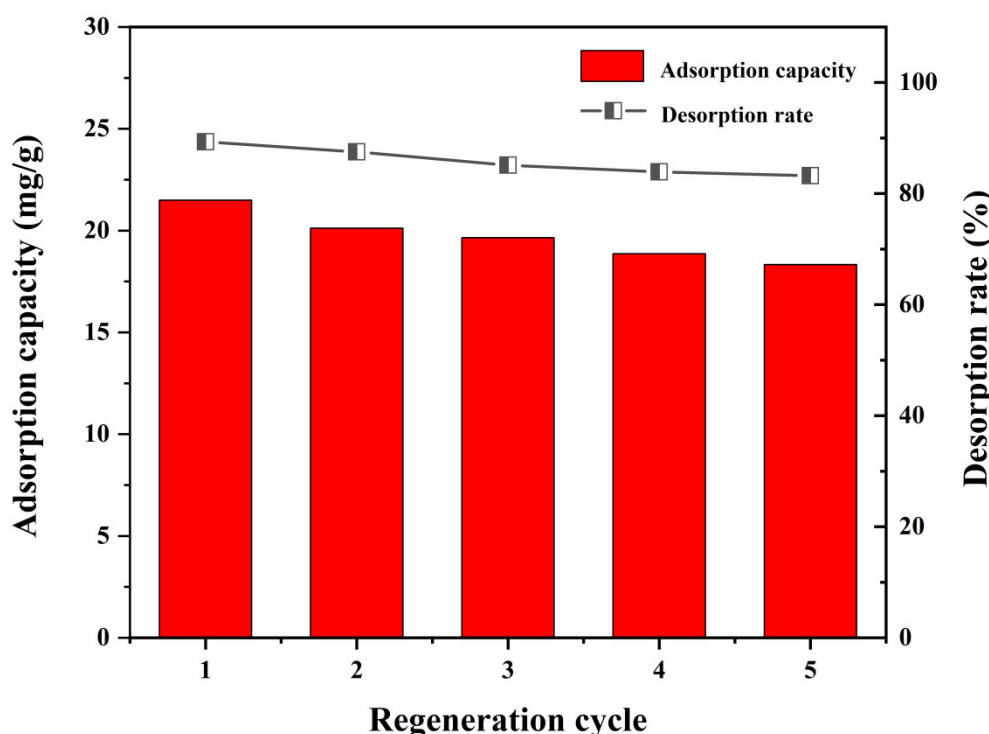


**Figure 10.** Variation of adsorption capacity and desorption rate by HNM-4 in regeneration cycle.

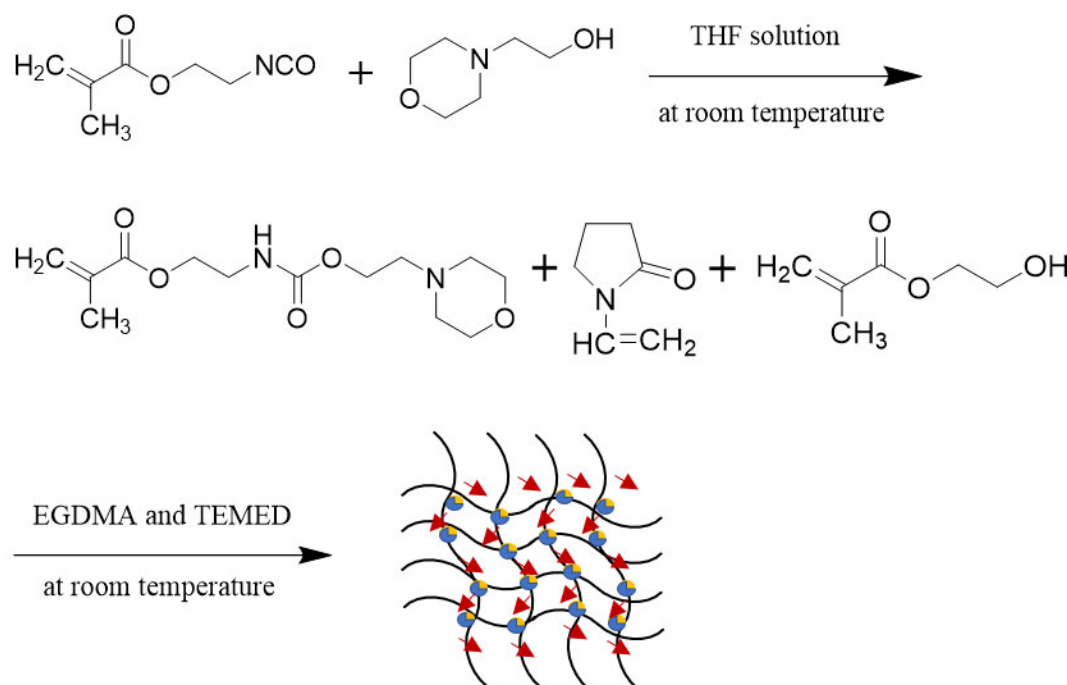
### 3. Experimental

#### 3.1. Materials

2-hydroxyethyl methacrylate (HEMA), N-vinylpyrrolidone (NVP), ethylene glycol dimethacrylate (EGDMA), potassium persulfate (KPS), N,N,N',N'-tetramethyl ethylenediamine (TEMED), 2-morpholine ethanol, isocyanooethyl methacrylate, and ethyl acetate were purchased from Shanghai Mac Ltd. All the aqueous solutions were prepared to use laboratory-prepared deionized water ( $0.055 \mu\Omega$ ). HNM Hydrogels were firstly prepared as a novel adsorbent for adsorption of  $\text{SO}_4^{2-}$ , as shown in Scheme 1.

#### 3.2. Preparation of 2-((2-Morpholineethoxy)carbonyl)amino)ethyl Methacrylate

The reaction was carried out by adding 5.33 g of 2-morpholine ethanol into a single-necked round-bottom flask, then adding 28 g of tetrahydrofuran to dissolve, and then adding 6.21 g of isocyanooethyl methacrylate, inserting a condenser tube, and stirring uniformly for 24 h at room temperature. After the reaction, the solution was recrystallized by adding petroleum ether, and the mixed liquid was poured into a filtering flask and filtered by rinsing with 1:1 ethyl acetate petroleum ether three times, and finally 2-((2-Morpholineethoxy)carbonyl)amino)ethyl methacrylate (MCAEM) was obtained by drying at room temperature.



**Scheme 1.** Schematic diagram of the synthesis of copolymer hydrogels.

### 3.3. Preparation of HNM Hydrogels

At room temperature, a certain amount of HEMA, NVP, and MCAEM were dissolved in deionized water to obtain the initial mixed solution, and the specific proportions of monomers are detailed in Table 4. Then, the initial mixed solution was transferred to an ice water bath, and EGDMA, KPS, and TEMED were added sequentially, with the amounts of EGDMA and KPS being 0.50 and 0.10 wt% of the total amount of monomers in the initial mixed solution, respectively, while the molar ratio of TEMED to KPS was 0.215. Then, the final mixed solution was slowly poured into a glass dish and subjected to free radical copolymerization at room temperature. The reaction was stopped after 24 h. The resulting hydrogel was immersed in deionized water, and the deionized water was changed every 12 h for 8 days to remove unreacted monomers. The prepared copolymer hydrogels were hydrogel sheets with a thickness of about 0.5 cm.

**Table 4.** The comonomer feed composition for synthesizing copolymer hydrogels.

Sample	HEMA (g)	NVP (g)	MCAEM (g)
HNM-1	4.75	4.75	0.00
HNM-2	4.75	4.75	2.00
HNM-3	4.75	4.75	3.00
HNM-4	4.75	4.75	4.00
HNM-5	4.75	4.75	5.00

### 3.4. Characterization

The FTIR spectra of the hydrogels were tested on an EQUINOX55 FTIR spectrometer (Bruker, Rheinstetten, Germany). The surface chemistry of the hydrogel surface was tested by XPS using an ESCA 5600 spectrometer (Perkin Elmer, Waltham, MA, USA) with an MgKa X-ray source (1253.6 eV), and the spectra were obtained at a take-off angle of 0°, obtaining measured spectra of the samples from 0 to 1200 eV. Scanning electron microscope (JEOL JSM-7800F, Tokyo, Japan) at an acceleration voltage of 10.0 kV was used to observe the surface morphology of the samples. The static contact angle of water droplets on the

surface of hydrogel sheets was measured at 25 °C using a contact angle goniometer (OCA 20, Dataphysics, Stuttgart, Germany). A 2 µL drop of water was carefully placed on the surface of the dissolved hydrogel sheet and then observed with an optical microscope to determine the static water contact angle of the test surface. The equilibrium water content of the hydrogels was determined at room temperature using the weight method. The hydrogels were placed in deionized water and absorbed, swelled, and weighed at specified time intervals until equilibrium was reached. Excess water was wiped off the surface of the hydrogels with wet filter paper, and the equilibrium wet weight was recorded. Subsequently, the hydrogel samples were dried to constant weight in a vacuum at 80 °C and weighed. The EWC of the hydrogel was calculated by the following equation:

$$\text{EWC} = \frac{(m_e - m_d)}{m_e} \times 100\%$$

where  $m_e$  is the saturated constant weight, and  $m_d$  is the dry constant weight.

A total of 1.000 g of analytical grade anhydrous sodium sulfate was weighed and then diluted to 1000 mL in a standard measuring flask to prepare a standard sulfate solution of 1000 ppm. A series of experimental sulfate solutions were prepared by diluting 5 mL, 10 mL, 15 mL, 20 mL, 25 mL, and 30 mL of the standard sulfate solution in six 100 mL volumetric flasks.

The hydrogels were tested for their sulfate ion adsorption capacity. A 0.5 cm × 0.5 cm hydrogel was added to 50 mL of 1000 mg/L  $\text{SO}_4^{2-}$  solution at room temperature and adsorbed in a constant temperature water bath at 25 °C with a shaking rate of 120 rpm for 3 h. The equilibrium concentration of sulfate in the water after adsorption experiments was determined using a UV-Vis spectrometer (PerkinElmer Lambda 35, Perkin Elmer, Waltham, MA, USA). The measurements were carried out at a maximum wavelength ( $\lambda_{\text{max}}$ ) of 420 nm [33,34].

The equilibrium adsorption amount ( $q_e$ ) of the hydrogel was calculated as follows:

$$q_e = \frac{(C_0 - C_e) \times V}{m}$$

where  $C_0$  (mg/L) and  $C_e$  (mg/L) are the initial and equilibrium concentrations of sulfate ions, respectively,  $m$  (g) is the mass of the hydrogel, and  $V$  (L) is the volume of the sulfate solution.

After ion adsorption, desorption experiments were carried out by replacing the equilibrium solutions with the same volume of 0.01 mol /L NaOH and shaking for 120 min. Sulfate concentrations in the extracts were measured by UV-spectrophotometric method. Repeat the adsorption–desorption process for 5 times.

The desorption rate was calculated as follows:

$$\eta = \frac{C_{\text{des}}V}{mq_e} \times 100\%$$

where  $C_{\text{des}}$  (mg/L) are the desorption concentrations of sulfate ions,  $m$  (g) is the mass of the hydrogel,  $V$  (L) is the volume of the KCl solution, and  $q_e$  (mg/g) is the equilibrium adsorption.

The point of zero charge (PZC) of the hydrogel was determined. A total of 2 g of hydrogel was stirred with 100 mL of 0.1 M potassium nitrate solution in a closed Erlenmeyer flask at 25 °C for 24 h to reach equilibrium. The initial pH (phi) was adjusted to a value between 2 and 12 by adding 0.1 M  $\text{HNO}_3$  or 0.1 M KOH solution. A plot of the final pH (phf) versus phi value was used to determine the PZC of the hydrogel.

The equilibrium adsorption of sulfate ions on the hydrogels was investigated at different pHs. The equilibrium adsorption amounts were measured and calculated after adding 0.5 cm × 0.5 cm hydrogels to 50 mL of 1000 mg/L  $\text{SO}_4^{2-}$  solutions of different pH at room temperature and adsorbed in a constant temperature water bath at 25 °C with a shaking rate of 120 rpm for 5 h. The pH values were adjusted by adding 0.1 mol/L HCl

and NaOH solutions ( $\text{pH} = 2, 4, 6, 8, 10$ , and  $12$ ). The equilibrium concentration of sulfate in water after the reaction was determined using a UV-Vis spectrometer.

The adsorption kinetics of the prepared obtained hydrogels were studied. A  $0.5 \text{ cm} \times 0.5 \text{ cm}$  hydrogel was added to  $50 \text{ mL}$  of  $300 \text{ mg/L}$   $\text{SO}_4^{2-}$  under certain pH conditions. The adsorption reaction was carried out in a constant temperature water bath at  $25^\circ\text{C}$  with a shaking rate of  $120 \text{ rpm}$ , and the adsorption amount was measured by aspirating the solution at certain times ( $t = 5, 10, 30, 60, 120, 240, 480$ , and  $720 \text{ min}$ ). The  $0.5 \text{ cm} \times 0.5 \text{ cm}$  hydrogels were added to  $50 \text{ mL}$  of different concentrations of  $\text{SO}_4^{2-}$  solution ( $C_0$  from  $5$  to  $300 \text{ mg/L}$ ) under optimum pH conditions. The adsorption was carried out in a constant temperature water bath at  $25^\circ\text{C}$  with a shaking rate of  $120 \text{ rpm}$  for  $3 \text{ h}$ . The equilibrium concentration of sulfate in the water after the reaction was determined using a UV-Vis spectrometer.

#### 4. Conclusions

In this study, a novel cationic MCAEM monomer was synthesized in one step from 2-morpholine ethanol, and a new cationic hydrogel was further prepared by polymerization with HEMA and NVP radicals to obtain a novel cationic hydrogel. The hydrogels were characterized by FTIR and XPS, and the results show that morpholine groups had been introduced into the hydrogels. The scanning electron microscopy characterization results show that when the morpholine group was introduced into the hydrogel, the surface of the hydrogel changed from micron-scale folds to nanoscale gaps, which increased the contact area with the solution. The EWC and contact angle of the hydrogels were tested, and it was found that as the content of the hydrophobic monomer MCAEM in the hydrogels increased, the equilibrium water content of the hydrogels increased, the static contact angle decreased, and the hydrophilicity increased. The factors affecting the adsorption performance of the hydrogels, such as the monomeric MCAEM content and the pH of the medium, were further investigated. It was found that the introduction of the MCAEM monomer in the hydrogel effectively improved the adsorption capacity of the hydrogel for sulfate ions, but the excessive content caused a slight decrease in the adsorption capacity. Moreover, the adsorption capacity of the hydrogel decreased as the solution pH value increased. Therefore, the adsorption capacity of the synthetic hydrogels for sulfate ions was higher in the acidic environment. The adsorption kinetics and isothermal parameters of the hydrogels were further investigated. The adsorption kinetics of hydrogels on sulfate ions followed more of a pseudo-secondary model, indicating that the rate control of the adsorption process was a chemical reaction process. According to the fitted calculations, the adsorption reaction process is more applicable to the Langmuir isotherm model to describe the adsorption process, which indicates that the adsorption of sulfate ions is monolayer. Adsorption–desorption experiments had shown that the hydrogels had excellent reusability. In summary, the results of this study indicate that the polyhydrogel system (HEMA–NVP–MCAEM) is advantageous in the removal of anionic sulfate ions from wastewater.

**Author Contributions:** Methodology, H.L., Y.J. and Z.W.; Formal analysis, W.C.; Investigation, G.Z.; Data curation, J.Z. and G.Z.; Writing – original draft, J.Z.; Writing – review & editing, Z.W.; Project administration, Y.J. and Z.W.; funding acquisition, J.Z., Y.J., G.Z. and Z.W. All authors have read and agreed to the published version of the manuscript.

**Funding:** This research was funded by the Lishui public welfare Technology Application Research Plan, grant number 2022GYX01, the Lishui public welfare Technology Application Research Plan, grant number 2021GYX01, the National Natural Science Foundation of China, grant number 21906041, the National Natural Science Foundation of China, grant number 21707060, the Scientific and Technological Project of Henan Province, grant number 192102110051, the Scientific and Technological Project of Henan Province, grant number 202102110123, the Zhejiang Province Basic Public Welfare Project, grant number LGF21B070001, the Lishui Public Welfare Technology Application Research Project, grant number 2021GYX13. And the APC was funded by the National Natural Science Foundation of China, grant number 21906041.

**Institutional Review Board Statement:** Not applicable.

**Informed Consent Statement:** Not applicable.

**Data Availability Statement:** Not applicable.

**Acknowledgments:** This work was financially supported by the project of National Natural Science Foundation of China (Grant No. 21906041 and 21707060), the Scientific and Technological Project of Henan Province (Grant No. 192102110051 and 202102110123), the Zhejiang Province Basic Public Welfare Project (Grant No. LGF21B070001), the Lishui public welfare Technology Application Research Plan (Grant No. 2022GYX01 and 2021GYX01) and Lishui Public Welfare Technology Application Research Project (Grant No. 2021GYX13). All individuals included in this section have consented to the Acknowledgments.

**Conflicts of Interest:** The authors declare no competing financial interest.

**Sample Availability:** Samples of the compounds are not available from the authors.

## References

1. Ao, H.; Cao, W.; Hong, Y.; Wu, J.; Wei, L. Adsorption of sulfate ion from water by zirconium oxide-modified biochar derived from pomelo peel. *Sci. Total. Environ.* **2019**, *708*, 135092. [[CrossRef](#)] [[PubMed](#)]
2. Pol, L.W.H.; Lens, P.N.L.; Stams, A.; Lettinga, G. Anaerobic treatment of sulphate-rich wastewaters. *Biodegradation* **1998**, *9*, 213–224. [[CrossRef](#)]
3. Amaral Filho, J.; Azevedo, A.; Etchepare, R.; Rubio, J. Removal of sulfate ions by dissolved air flotation (DAF) following precipitation and flocculation. *Int. J. Miner. Process.* **2016**, *149*, 1–8. [[CrossRef](#)]
4. Ragoug, R.; Metalssi, O.O.; Barberon, F.; Torrenti, J.-M.; Roussel, N.; Divet, L.; de Lacaillerie, J.-B.D. Durability of cement pastes exposed to external sulfate attack and leaching: Physical and chemical aspects. *Cem. Concr. Res.* **2018**, *116*, 134–145. [[CrossRef](#)]
5. Mark, A.; Hans, B. Durability, service life prediction and modelling for reinforced concrete structures review and critique. *Cem. Concr. Res.* **2019**, *122*, 17–29.
6. Hassan, W.; Faisal, A.; Abed, E.; Al-Ansari, N.; Saleh, B. New Composite Sorbent for Removal of Sulfate Ions from Simulated and Real Groundwater in the Batch and Continuous Tests. *Molecules* **2021**, *26*, 4356. [[CrossRef](#)]
7. Józwiak, T.; Mielcarek, A.; Janczukowicz, W.; Rodziewicz, J.; Majkowska-Gadomska, J.; Chojnowska, M. Hydrogel chitosan sorbent application for nutrient removal from soilless plant cultivation wastewater. *Environ. Sci. Pollut. Res.* **2018**, *25*, 18484–18497. [[CrossRef](#)]
8. Alsbaijee, A.; Smith, B.J.; Xiao, L.; Ling, Y.; Helbling, D.E.; Dichtel, W.R. Rapid removal of organic micropollutants from water by a porous beta-cyclodextrin polymer. *Nature* **2016**, *529*, 190–194. [[CrossRef](#)]
9. Chen, Y.; Yan, J.; Zhang, Y.; Chen, W.; Wang, Z.; Wang, L. Synthesis, Characterization and Antibacterial Activity of Novel β-cyclodextrin Polyurethane Materials. *J. Polym. Environ.* **2021**, *30*, 1012–1027. [[CrossRef](#)]
10. Ying, T.; Su, J.; Jiang, Y.; Ni, L.; Jiang, X.; Ke, Q.; Xu, H. Superhydrophobic MOFs decorated on hierarchically micro/nanofibrous membranes for high-performance emulsified oily wastewater separation and cationic dyes adsorption. *J. Mater. Chem. A* **2022**, *10*, 829–845. [[CrossRef](#)]
11. Noreen, S.; Tahira, M.; Ghamkhar, M.; Hafiz, I.; Bhatti, H.N.; Nadeem, R.; Murtaza, M.A.; Yaseen, M.; Sheikh, A.A.; Naseem, Z.; et al. Treatment of textile wastewater containing acid dye using novel polymeric graphene oxide nanocomposites (GO/PAN, GO/PPy, GO/PSty). *J. Mater. Res. Technol.* **2021**, *14*, 25–35. [[CrossRef](#)]
12. Rad, L.R.; Anbia, M. Zeolite-based composites for the adsorption of toxic matters from water: A review. *J. Environ. Chem. Eng.* **2021**, *9*, 106088. [[CrossRef](#)]
13. Mo, Z.; Tai, D.; Zhang, H.; Shahab, A. A comprehensive review on the adsorption of heavy metals by zeolite imidazole framework (ZIF-8) based nanocomposite in water. *Chem. Eng. J.* **2022**, *443*, 136320. [[CrossRef](#)]
14. Rego, R.M.; Kuriya, G.; Kurkuri, M.D.; Kigga, M. MOF based engineered materials in water remediation: Recent trends. *J. Hazard. Mater.* **2021**, *403*, 123605. [[CrossRef](#)]
15. Ilgin, P.; Ozay, O. Novel stimuli-responsive hydrogels derived from morpholine: Synthesis, characterization and absorption uptake of textile azo dye. *Iran. Polym. J.* **2017**, *26*, 391–404. [[CrossRef](#)]
16. Prabhakar, M.N.; Sudhakara, P.; Subha, M.C.S.; Rao, K.C.; Song, J. Novel thermoresponsive biodegradable nanocomposite hydrogels for dual function in biomedical applications. *Polym. Plast. Technol. Eng.* **2015**, *54*, 1704–1714. [[CrossRef](#)]
17. Gao, C.; Ren, J.; Zhao, C.; Kong, W.; Dai, Q.; Chen, Q.; Liu, C.; Sun, R. Xylan-based temperature/pH sensitive hydrogels for drug controlled release. *Carbohydr. Polym.* **2016**, *151*, 189–197. [[CrossRef](#)]
18. Clara, I.; Lavanya, R.; Natchimuthu, N. pH and temperature responsive hydrogels of poly(2-acrylamido-2-methyl-1-propanesulfonic acid-co-methacrylic acid): Synthesis and swelling characteristics. *J. Macromol. Sci. A* **2016**, *53*, 492–499. [[CrossRef](#)]
19. Ozay, O.; Ozay, H. Separation and speciation of iron ions by using colorimetric hydrogels. *J. Macromol. Sci. Pure Appl. Chem.* **2014**, *51*, 308–317. [[CrossRef](#)]
20. Ozay, H.; Ozay, O. Rhodamine based reusable and colorimetric naked-eye hydrogel sensors for Fe<sup>3+</sup> ion. *Chem. Eng. J.* **2013**, *232*, 364–371.

21. Fang, R.; He, W.; Xue, H.; Chen, W. Synthesis and characterization of a high-capacity cationic hydrogel adsorbent and its application in the removal of acid black 1 from aqueous solution. *React. Funct. Polym.* **2016**, *102*, 1–10. [[CrossRef](#)]
22. Ladopoulou, E.M.; Matralis, A.N.; Nikitakis, A.; Kourounakis, A.P. Antihyperlipidemic morpholine derivatives with antioxidant activity: An investigation of the aromatic substitution. *Bioorg. Med. Chem.* **2015**, *23*, 7015–7023. [[CrossRef](#)] [[PubMed](#)]
23. Dhahagani, K.; Kumar, S.M.; Chakkaravarthi, G.; Anitha, K.; Rajesh, J.; Ramu, A.; Rajagopal, G. Synthesis and spectral characterization of Schiff base complexes of Cu(II), Co(II), Zn(II) and VO(IV) containing 4-(4-aminophenyl)morpholine derivatives: Antimicrobial evaluation and anticancer studies. *Spectrochim. Acta Part A Mol. Biomol. Spectrosc.* **2014**, *117*, 87–94. [[CrossRef](#)] [[PubMed](#)]
24. Kilic, A.; Tas, E.; Gumgum, B.; Yilmaz, I. Synthesis, spectroscopic and electrochemical investigations of two vic-dioximes and their mononuclear Ni(II), Cu(II) and Co(II) metal complexes containing morpholine group. *Chin. J. Chem.* **2006**, *24*, 1599–1604. [[CrossRef](#)]
25. Burat, A.K.; Koca, A.; Lewtak, J.P.; Gryko, D.T. Preparation, electrochemistry and optical properties of unsymmetrical phthalocyanines bearing morpholine and tert-butylphenoxy substituents. *Synth. Met.* **2011**, *161*, 1537–1545. [[CrossRef](#)]
26. Rocha, L.R.; D'Elia, E.; Medeiros, R.A.; Tarley, C.R.T. Electroanalytical Determination of Morpholine as a Corrosion Inhibitor at a Cathodically Pretreated Boron-Doped Diamond Electrode. *Anal. Lett.* **2018**, *52*, 1083–1096. [[CrossRef](#)]
27. Shin, Y.; Choi, M.Y.; Choi, J.; Na, J.H.; Kim, S.Y. Design of an Electro-Stimulated Hydrogel Actuator System with Fast Flexible Folding Deformation under a Low Electric Field. *ACS Appl. Mater. Interfaces* **2021**, *13*, 15633–15646. [[CrossRef](#)]
28. Fathy, M.; Moghny, T.A.; Awadallah, A.E.; El-Bellahi, A.-H.A.-A. Study the adsorption of sulfates by high cross-linked polystyrene divinylbenzene anion-exchange resin. *Appl. Water Sci.* **2014**, *7*, 309–313. [[CrossRef](#)]
29. Gu, B.; Ku, Y.-K.; Jardine, P.M. Sorption and Binary Exchange of Nitrate, Sulfate, and Uranium on an Anion-Exchange Resin. *Environ. Sci. Technol.* **2017**, *38*, 3184–3188. [[CrossRef](#)]
30. El-Sigeny, S.; Mohamed, S.K.; Abou Taleb, M.F. Radiation synthesis and characterization of styrene/acrylic acid/organophilic montmorillonite hybrid nanocomposite for sorption of dyes from aqueous solutions. *Polym. Compos.* **2014**, *35*, 2353–2364. [[CrossRef](#)]
31. Mahdavinia, R.G.; Aghaie, H.; Sheykholie, H.; Vadini, M.T.; Etemadi, H. Synthesis of CarAlg/MMt nanocomposite hydrogels and adsorption of cationic crystal violet. *Carbohydr. Polym.* **2013**, *98*, 358–365. [[CrossRef](#)]
32. Sun, P.; Hui, C.; Khan, R.A.; Du, J.; Zhang, Q.; Zhao, Y.-H. Efficient removal of crystal violet using Fe3O4-coated biochar: The role of the Fe3O4 nanoparticles and modeling study their adsorption behavior. *Sci. Rep.* **2015**, *5*, 12638. [[CrossRef](#)]
33. Solińska, A.; Bajda, T. Modified zeolite as a sorbent for removal of contaminants from wet flue gas desulphurization wastewater. *Chemosphere* **2022**, *286*, 131772. [[CrossRef](#)]
34. Hudaib, B. Treatment of real industrial wastewater with high sulfate concentrations using modified Jordanian kaolin sorbent: Batch and modelling studies. *Heliyon* **2021**, *7*, e08351. [[CrossRef](#)]

**Disclaimer/Publisher's Note:** The statements, opinions and data contained in all publications are solely those of the individual author(s) and contributor(s) and not of MDPI and/or the editor(s). MDPI and/or the editor(s) disclaim responsibility for any injury to people or property resulting from any ideas, methods, instructions or products referred to in the content.